CHAPTER 5

MHD CARREAU FLUID FLOW OVER NONLINEAR STRETCHING SHEET

Content of this chapter is accepted in:

International Journal of Applied and Computational Mathematics

2022 **(Springer) (Scopus)**

Chapter 5

MHD Carreau fluid flow over nonlinear stretching sheet

Mathematically, the non-Newtonian behaviour of blood in narrow arteries is examined by treating the blood as a Carreau fluid. Stretching a sheet facilitates heat and mass transfer, which has numerous applications in the polymer sector, including lamination, spinning fibres, and other processes.

5.1 Introduction of the Problem

Because of the distinct properties, nature contains a plethora of non-Newtonian substances. The majority of the fluids are non-Newtonian in nature, means The resistance of a non-Newtonian fluid varies with the rate of shear strain. Carreau et al. [102] developed a model where fluid viscosity is dependent on the shear rate. Madhu et al. [78] addressed MHD Carreau fluid flow with heat transfer. Nazir et al. [134] explores the transport phenomenon of temperature dependent diffusion coefficients in Carreau fluid.

Extrusion, glass blowing, hot rolling, the production of plastic and rubber sheets, the growth of crystals, continuous cooling, and fibre spinning are just a few manufacturing processes that largely rely on the understanding of flow and heat transmission caused by a stretching sheet. Siddheshwar et al. [104, 105] studied a stretching sheet problem involving different types of MHD fluid flow. Aslani et al. [53] explored MHD micropolar fluid flow with radiation. Mabood et al. [30] analyzed nonlinear radiation effects on MHD fluid flow. Hussain et al. [71] found the significance of nonlinear radiation and convective boundary conditions on MHD Casson fluid flow. Nonlinear radiation effect on Williamson fluid flow is evaluated by Bibi et al. [65]. Gireesha et al. [21, 22] scrutinized nonlinear radiation impact on various fluid flow with heat transfer. Gupta et al. [118] analyzed nonlinear radiation impact on 2D

Williamson fluid flow. Ullah et al. [19] explained non-linear thermal radiation impact on Carreau fluid flow. Mahabaleshwar et al. [133] scrutinized impact of slip condition on liquid flow. Ajibade and Umar [1] studied viscous dissipation impact on an incompressible viscous fluid flow with varying viscosity. Radiation impact on flow of Carreau liquid with varying viscosity is analyzed by Sultan et al. [31]. Dada and Onwubuoya [67] investigated thermal conductivity and varying viscosity impact on Williamson fluid flow. Idowu et al. [11] explored effect of variable viscosity on MHD Natural convective heat and mass transfer flow of Casson fluid.

5.2 Novelty of the Chapter

Purpose of this chapter is to investigate analytic solution of Soret and Duour effects on MHD Carreau fluid flow over stretching/Shrinking sheet considering variable visocity. Solution of the problem is found by Homotopy analysis method.

5.3 Mathematical Formulation of the Problem

Consider $2D$ steady, incompressible MHD Carreau fluid flow over a shrinking or stretching sheet is considered. Stretching/shrinking sheet is taken along x axis. Magnetic field $\mathcal{B} = B_0 x^{\frac{m-1}{2}}$ is implemented perpendicular to the surface, where $U_w(x) = a^* x^m$ and $U_e(x) = b^* x^m$. Non-linear thermal radiation, Soret and Dufour effects are taken into account.
The basic equations of MHD are given by

$$\nabla \cdot V = 0, \tag{5.3.1}$$

$$\rho \frac{dV}{dt} = \nabla \cdot S + F_L \tag{5.3.2}$$

$$\left(\frac{dT}{dt}\right) = \frac{1}{\rho C_p}\nabla \cdot (\kappa \nabla T) - \frac{1}{\rho C_p}\nabla \cdot q_r + \nabla \cdot \left(\frac{D_M K_T}{C_p C_s}\nabla C\right), \tag{5.3.3}$$

$$\frac{dC}{dt} = \nabla \cdot (D_M \nabla C) + \nabla \cdot \left(\frac{D_M K_T}{T_m}\nabla T\right), \tag{5.3.4}$$

where F_L is consisting the Lorentz force described as

$$F_L = J \times \mathcal{B} \tag{5.3.5}$$

and $J = \sigma\,(E + V \times \mathcal{B})$, now if we consider $E = 0$, then $J = \sigma\,(V \times \mathcal{B})$.

Now, Continuity Eq. (5.3.1) simplified as:

$$\frac{\partial u}{\partial x}+\frac{\partial v}{\partial y}=0, \tag{5.3.6}$$

Now, stress tensors are given as

$$\tau_{xx}=2\mu^*\frac{\partial u}{\partial x}\left(1+\Gamma^2\left(\frac{p_i-1}{2}\right)\left(\frac{\partial u}{\partial y}\right)^2\right),\quad \tau_{yy}=2\mu^*\frac{\partial v}{\partial y}\left(1+\Gamma^2\left(\frac{p_i-1}{2}\right)\left(\frac{\partial u}{\partial y}\right)^2\right), \tag{5.3.7}$$

$$\tau_{yx}=\tau_{xy}=\mu^*\left(\frac{\partial u}{\partial y}+\frac{\partial v}{\partial x}\right)\left(1+\Gamma^2\left(\frac{p_i-1}{2}\right)\left(\frac{\partial u}{\partial y}\right)^2\right). \tag{5.3.8}$$

then,

$$\begin{aligned}\rho\left(u\frac{\partial u}{\partial x}+v\frac{\partial u}{\partial y}\right)&=-\frac{\partial P}{\partial x}+\frac{\partial \tau_{xy}}{\partial y}+\frac{\partial \tau_{xx}}{\partial x}-\sigma\mathcal{B}^2u,\\ \rho\left(u\frac{\partial v}{\partial x}+v\frac{\partial v}{\partial y}\right)&=-\frac{\partial P}{\partial y}+\frac{\partial \tau_{yy}}{\partial y}+\frac{\partial \tau_{yx}}{\partial x},\end{aligned} \tag{5.3.9}$$

In polar coordiantes, Eq. (5.3.2) simplified as below,

$$\begin{aligned}u\frac{\partial u}{\partial x}+v\frac{\partial u}{\partial y}=\frac{1}{\rho}\frac{\partial}{\partial y}\left(\mu^*(T)\frac{\partial u}{\partial y}\right)-\frac{1}{\rho}\frac{\partial P}{\partial x}+3\frac{\mu^*(T)}{\rho}\left(\frac{p_i-1}{2}\right)\Gamma^2\left(\frac{\partial u}{\partial y}\right)^2\frac{\partial^2u}{\partial y^2}\\ +\frac{1}{\rho}\left(\frac{p_i-1}{2}\right)\Gamma^2\frac{\partial\mu^*(T)}{\partial y}\left(\frac{\partial u}{\partial y}\right)^3-\frac{\sigma\mathcal{B}^2}{\rho}u,\end{aligned} \tag{5.3.10}$$

because the flow field is uniform at a suitably large distance from the edge surface, so in the free stream $u=U_e=b^*x^m$, then the Eq. (5.3.10) reduced to

$$\frac{1}{\rho}\frac{\partial P}{\partial x}=-U_e\frac{dU_e}{dx}-\frac{\sigma\mathcal{B}^2}{\rho}U_e, \tag{5.3.11}$$

eliminating $\frac{\partial P}{\partial x}$ in Eq. (5.3.10) by using Eq. (5.3.11), we finally obtain

$$\begin{aligned}u\frac{\partial u}{\partial x}+v\frac{\partial u}{\partial y}=U_e\frac{dU_e}{dx}+\frac{\sigma\mathcal{B}^2}{\rho}U_e+\frac{1}{\rho}\frac{\partial}{\partial y}\left(\mu^*(T)\frac{\partial u}{\partial y}\right)+3\frac{\mu^*(T)}{\rho}\left(\frac{p_i-1}{2}\right)\Gamma^2\left(\frac{\partial u}{\partial y}\right)^2\frac{\partial^2u}{\partial y^2}\\ +\frac{1}{\rho}\left(\frac{p_i-1}{2}\right)\Gamma^2\frac{\partial\mu^*(T)}{\partial y}\left(\frac{\partial u}{\partial y}\right)^3-\frac{\sigma\mathcal{B}^2}{\rho}u,\end{aligned} \tag{5.3.12}$$

reduced form of energy and concentration equations (5.3.3) and (5.3.4) are

$$u\frac{\partial T}{\partial x}+v\frac{\partial T}{\partial y}+\frac{1}{\rho C_p}\frac{\partial q_r}{\partial y}-\frac{\kappa}{\rho C_p}\frac{\partial^2 T}{\partial y^2}-\frac{D_M K_T}{C_p C_s}\frac{\partial^2 C}{\partial y^2}=0, \tag{5.3.13}$$

$$u\frac{\partial C}{\partial x}+v\frac{\partial C}{\partial y}-\frac{D_M K_T}{T_m}\frac{\partial^2 T}{\partial y^2}-D_M\frac{\partial^2 C}{\partial y^2}=0, \tag{5.3.14}$$

Now, continuity equation is

$$\frac{\partial u}{\partial x}+\frac{\partial v}{\partial y}=0, \tag{5.3.15}$$

Momentum equation is

$$u\frac{\partial u}{\partial x}+v\frac{\partial u}{\partial y}-U_e\frac{dU_e}{dx}-\frac{1}{\rho}\frac{\partial}{\partial y}\left(\mu^*(T)\frac{\partial u}{\partial y}\right)-3\frac{\mu^*(T)}{\rho}\left(\frac{p_i-1}{2}\right)\Gamma^2\left(\frac{\partial u}{\partial y}\right)^2\frac{\partial^2 u}{\partial y^2}$$
$$-\frac{1}{\rho}\left(\frac{p_i-1}{2}\right)\Gamma^2\frac{\partial \mu^*(T)}{\partial y}\left(\frac{\partial u}{\partial y}\right)^3-\frac{\sigma\mathcal{B}^2}{\rho}\left(U_e-u\right)=0, \tag{5.3.16}$$

Energy equation is

$$u\frac{\partial T}{\partial x}+v\frac{\partial T}{\partial y}+\frac{1}{\rho C_p}\frac{\partial q_r}{\partial y}-\frac{\kappa}{\rho C_p}\frac{\partial^2 T}{\partial y^2}-\frac{D_M K_T}{C_p C_s}\frac{\partial^2 C}{\partial y^2}=0, \tag{5.3.17}$$

Concentration equation is

$$u\frac{\partial C}{\partial x}+v\frac{\partial C}{\partial y}-\frac{D_M K_T}{T_m}\frac{\partial^2 T}{\partial y^2}-D_M\frac{\partial^2 C}{\partial y^2}=0, \tag{5.3.18}$$

to the boundary conditions

$$\left.\begin{aligned} u=U_w(x),\ v=\ v_w(x),\ \ C=C_w,\ \frac{\partial T}{\partial y}=-\frac{q_0}{\kappa}x^{\frac{m-1}{2}},\ \text{at } y=0,\\ u=U_e(x),\ \ C\to C_\infty,\ \ T\to T_\infty,\ \text{as } y\to\infty. \end{aligned}\right\} \tag{5.3.19}$$

Heat flux by Rosseland [126] is:

$$q_r=-\frac{4\sigma^*\partial T^4}{3k^*\partial y} \tag{5.3.20}$$

expanding T^4 beyond the first degree in $(T-T_\infty)$ with the help of the Taylor series about T_∞ and discard higher order terms, we get

$$T^4+3T_\infty^4-4TT_\infty^3\cong 0.$$

then,

$$q_r = -\frac{16\sigma^* T_\infty^3}{3k^*}\frac{\partial T}{\partial y} \tag{5.3.21}$$

Linear radiative heat flux is represented by the equation (5.3.21). However, the intention of this research is to explore the effect of nonlinear radiation, so by changing T_∞^3 with T^3 in Eq.(5.3.21), we get

$$q_r = -\frac{16\sigma^* T^3}{3k^*}\frac{\partial T}{\partial y} \tag{5.3.22}$$

Adegbie et al. [112] provide a mathematical model of temperature dependent viscosity

$$\mu\left(T\right) = \mu^*\left[1 + h_1\left(T_\infty - T\right)\right], \tag{5.3.23}$$

where, h_1 is constant and its value depends on the fluid.
The introduction of similarity transformations

$$\left.\begin{aligned} u = b^* x^m f'\left(\eta\right), \quad v = -\sqrt{b^*\nu}\, x^{\frac{m-1}{2}}\left[\left(\frac{m-1}{2}\right)\eta f'\left(\eta\right) + \left(\frac{m+1}{2}\right) f\left(\eta\right)\right], \\ \eta = \sqrt{\frac{b^*}{\nu}}\, y x^{\frac{m-1}{2}}, \quad \phi\left(\eta\right) = \frac{C - C_\infty}{C_w - C_\infty}, \quad \theta\left(\eta\right) = \sqrt{\frac{b^*}{\nu}}\frac{\kappa}{q_0}(T - T_\infty), \end{aligned}\right\} \tag{5.3.24}$$

Inserting Eq. (5.3.24) in Eqs. (5.3.15)-(5.3.18) and (5.3.19), Equation (5.3.15) is identically satisfied and Eqs. (5.3.16)-(5.3.18) and (5.3.19) will be

$$\begin{aligned} (1-\zeta\theta)\left[1 + 3\left(\frac{p_i - 1}{2}\right) We^2 f'' f''\right] f''' - m(f'f' - 1) - M^2(f' - 1) \\ - \zeta\left[1 + \left(\frac{p_i - 1}{2}\right) We^2 f'' f''\right] f''\theta' + \left(\frac{1+m}{2}\right) f f'' = 0, \end{aligned} \tag{5.3.25}$$

$$\begin{aligned} \left(1 + \frac{4}{3} Rd\left\{\left(\theta_w - 1\right)\theta + 1\right\}^3\right)\theta'' + DuPr\phi'' + 4Rd\left(\left(\theta_w - 1\right)\theta + 1\right)^2\left(\theta_w - 1\right)\theta'\theta' \\ + Pr\left(\frac{m+1}{2}\right)\theta' f = 0, \end{aligned} \tag{5.3.26}$$

$$\phi'' + \frac{m+1}{2} Scf\phi' + ScSr\theta'' = 0, \tag{5.3.27}$$

$$f\left(\eta\right) = f_w, \; f'\left(\eta\right) = B, \; \theta'\left(\eta\right) = -1, \; \phi\left(\eta\right) = 1, \quad \text{at} \quad \eta = 0, \tag{5.3.28}$$

$$f'\left(\eta\right) = 1, \; \theta\left(\eta\right) = \; \phi\left(\eta\right) = 0. \quad \text{as} \quad \eta \to \infty. \tag{5.3.29}$$

here We, B, M, f_w, θ_w, ζ, Du, Sr, Pr and Sc are given as $We = \sqrt{\frac{\Gamma^2 b^{*3} x^{3m-1}}{\nu}}$, $B = \frac{a^*}{b^*}$, $M = \sqrt{\frac{\sigma B_0^2}{\rho b^*}}$, $f_w = \frac{-2v_w}{\sqrt{b^*\nu}x^{\frac{m-1}{2}}(m+1)}$, $\theta_w = 1+\sqrt{\frac{\nu}{b^*}}\frac{q_0}{\kappa}\frac{1}{T_\infty}$, $\zeta = h_1\sqrt{\frac{\nu}{b^*}}\frac{q_0}{\kappa}$, $Pr = \frac{\mu C_p}{\kappa}$,$Sc = \frac{\nu}{D_M}$, $Rd = \frac{4\sigma^* T_\infty^3}{k^*\kappa}$, $Du = \frac{D_M K_T}{\nu C_p C_s}\frac{(C_w - C_\infty)}{\sqrt{\frac{\nu}{b^*}}\frac{q_0}{\kappa}}$, $Sr = \frac{D_M K_T}{\nu T_m}\frac{\sqrt{\frac{\nu}{b^*}}\frac{q_0}{\kappa}}{(C_w - C_\infty)}$,

Skin friction coefficient C_{fx}, Nusselt count Nu_x and Sherwood count Sh_x are the physical measures of concern in this study, and they are described as,

$$C_{fx} = \tau_w(x)\,\rho U_e^2, \tag{5.3.30}$$

$$\text{where, surface shear stress } \tau_w(x) = \mu(T)\left\{1 + 3\Gamma^2\left(\frac{p_i - 1}{2}\right)\left(\frac{\partial u}{\partial y}\right)^2\right\}\frac{\partial u}{\partial y}\bigg|_{y=0}, \tag{5.3.31}$$

$$\text{then } C_f Re_x^{\frac{1}{2}} = (1 - \zeta\theta(0))\left[1 + 3\left(\frac{p_i - 1}{2}\right)We^2 f''(0) f''(0)\right] f''(0), \tag{5.3.32}$$

$$Nu_x = \frac{x q_w(x)}{\kappa(T - T_\infty)}, \tag{5.3.33}$$

$$\text{where, surface heat flux } q_w(x) = \left(-\kappa\frac{\partial T}{\partial y} + q_r\right)_{y=0} \tag{5.3.34}$$

$$\text{then } Nu_x Re_x^{-\frac{1}{2}} = \frac{\left(1 + \frac{4}{3}Rd\left\{(\theta_w - 1)\theta(0) + 1\right\}^3\right)}{\theta(0)}, \tag{5.3.35}$$

$$Sh_x = \frac{x q_m}{D_M(C_w - C_\infty)}, \text{ where surface mass flux } q_m = -D_M\frac{\partial C}{\partial y}\bigg|_{y=0}, \tag{5.3.36}$$

$$\text{then } Sh_x Re_x^{-\frac{1}{2}} = -\phi'(0), \tag{5.3.37}$$

where $Re_x^{\frac{1}{2}} = \sqrt{\frac{b^*}{\nu}}x^{\frac{m+1}{2}}$.

5.4 Solution by Homotopy Analysis Method

Liao [121] established HAM. Initial guesses and linear operators are described in that kind of a manner that they gratify the boundary conditions given in Eq. (5.3.19).

Initial guesses

$$f_0(\eta) = \eta + (f_w + B - 1) + (1 - B)\, e^{-\eta}, \quad \theta_0(\eta) = e^{-\eta}, \quad \phi_0(\eta) = e^{-\eta}, \tag{5.4.1}$$

and linear operators

$$\mathcal{L}_f = \frac{\partial^3 f}{\partial \eta^3} + \frac{\partial^2 f}{\partial \eta^2}, \quad \mathcal{L}_\theta = \frac{\partial^2 \theta}{\partial \eta^2} + \frac{\partial \theta}{\partial \eta}, \quad \mathcal{L}_\phi = \frac{\partial^2 \phi}{\partial \eta^2} + \frac{\partial \phi}{\partial \eta}, \tag{5.4.2}$$

Satisfying

$$\mathcal{L}_f\left(k_1 + k_2\eta + k_3 e^{-\eta}\right) = 0, \mathcal{L}_\theta\left(k_4 + k_5 e^{-\eta}\right) = 0, \mathcal{L}_\phi\left(k_6 + k_7 e^{-\eta}\right) = 0. \tag{5.4.3}$$

where arbitrary constants are k_i, $(i = 1,\ 2, \ldots, 7)$.

5.4.1 Zero-th order deformation

$$(1 - q)\, \mathcal{L}_f\left[F(\eta; q) - f_0(\eta)\right] = q\hbar_f \mathcal{N}_f\left[F(\eta; q)\right], \tag{5.4.4}$$

$$(1 - q)\, \mathcal{L}_\theta\left[\Theta(\eta; q) - \theta_0(\eta)\right] = q\hbar_\theta N_\theta\left[\Theta(\eta; q)\right], \tag{5.4.5}$$

$$(1 - q)\, \mathcal{L}_\phi\left[\Phi(\eta; q) - \phi_0(\eta)\right] = q\hbar_\phi \mathcal{N}_\phi\left[\Phi(\eta; q)\right]. \tag{5.4.6}$$

where $q \in [0, 1]$ and non-zero auxiliary parameters are $\hbar_f, \hbar_\theta, \hbar_\phi$.

$$\mathcal{N}_F\left[F(\eta; q)\right] = (1 - \zeta\Theta)\left[1 + 3\left(\frac{p_i - 1}{2}\right) We^2 \frac{\partial^2 F}{\partial \eta^2}\frac{\partial^2 F}{\partial \eta^2}\right]\frac{\partial^3 F}{\partial \eta^3} - M^2\left(\frac{\partial F}{\partial \eta} - 1\right)$$
$$-m\left(\frac{\partial F}{\partial \eta}\frac{\partial F}{\partial \eta} - 1\right) - \zeta\left[1 + \left(\frac{p_i - 1}{2}\right) We^2 \frac{\partial^2 F}{\partial \eta^2}\frac{\partial^2 F}{\partial \eta^2}\right]\frac{\partial^2 F}{\partial \eta^2}\frac{\partial \Theta}{\partial \eta} + \left(\frac{m + 1}{2}\right) F\frac{\partial^2 F}{\partial \eta^2}, \tag{5.4.7}$$

$$\mathcal{N}_\theta\left[\Theta(\eta; q)\right] = \left(1 + \frac{4}{3}Rd\left\{1 + (\theta_w - 1)\,\Theta\right\}^3\right)\frac{\partial^2 \Theta}{\partial \eta^2} + Pr\left(\frac{m + 1}{2}\right) F\frac{\partial \Theta}{\partial \eta}$$
$$+ DuPr\frac{\partial^2 \Phi}{\partial \eta^2} + 4Rd\left(1 + (\theta_w - 1)\,\Theta\right)^2 (\theta_w - 1)\left(\frac{\partial \Theta}{\partial \eta}\right)^2, \tag{5.4.8}$$

$$\mathcal{N}_\phi\left[\Phi(\eta; q)\right] = \frac{\partial^2 \Phi}{\partial \eta^2} + Sc\left(\frac{m + 1}{2}\right) F\frac{\partial \Phi}{\partial \eta} + ScSr\frac{\partial^2 \Theta}{\partial \eta^2}, \tag{5.4.9}$$

boundary conditions subject to

$$F'(0;q) = B, \quad F(0;q) = f_w, \quad \Phi(0;q) = 1, \quad \Theta'(0;q) = -1, \tag{5.4.10}$$

$$F'(+\infty;q) = 1, \quad \Phi(+\infty;q) = 0, \quad \Theta(+\infty;q) = 0. \tag{5.4.11}$$

where

$$F(\eta;0) = f_0(\eta), \quad \Theta(\eta;0) = \theta_0(\eta), \quad \Phi(\eta;0) = \phi_0(\eta), \tag{5.4.12}$$

$$F(\eta;1) = f(\eta), \quad \Theta(\eta;1) = \theta(\eta), \quad \Phi(\eta;1) = \phi(\eta), \tag{5.4.13}$$

If q is vary from 0 to 1, then we get

$$F(\eta;q) = f_0(\eta) + \sum_{i=1}^{\infty} f_i(\eta)\, q^i, \tag{5.4.14}$$

$$\Theta(\eta;q) = \theta_0(\eta) + \sum_{i=1}^{\infty} \theta_i(\eta)\, q^i, \tag{5.4.15}$$

$$\Phi(\eta;q) = \phi_0(\eta) + \sum_{i=1}^{\infty} \phi_i(\eta)\, q^i. \tag{5.4.16}$$

where

$$f_i(\eta) = \frac{1}{i!}\frac{\partial^i f(\eta;q)}{\partial \eta^{\,i}}\bigg|_{q=0}, \ \theta_i(\eta) = \frac{1}{i!}\frac{\partial^i \theta(\eta;q)}{\partial \eta^{\,i}}\bigg|_{q=0}, \ \phi_i(\eta) = \frac{1}{i!}\frac{\partial^i \phi(\eta;q)}{\partial \eta^{\,i}}\bigg|_{q=0} \tag{5.4.17}$$

The convergence of the series is largely reliant on $\hbar_f$, $\hbar_\theta$ and $\hbar_\phi$. If non-zero $\hbar_f$, $\hbar_\theta$ and $\hbar_\phi$ are selected in such a manner that Equation (5.4.16) converge at $q = 1$.

$$f(\eta) = f_0(\eta) + \sum_{i=1}^{\infty} f_i(\eta), \ \theta(\eta) = \theta_0(\eta) + \sum_{i=1}^{\infty} \theta_i(\eta), \ \phi(\eta) = \phi_0(\eta) + \sum_{i=1}^{\infty} \phi_i(\eta) \tag{5.4.18}$$

5.4.2 i-th order deformation

The i^{th} order deformation equations are

$$\left.\begin{aligned} \mathcal{L}_f[f_i(\eta) - \chi_i f_{i-1}(\eta)] &= \hbar_f \mathcal{R}_{f,i}(\eta), \\ \mathcal{L}_\theta[\theta_i(\eta) - \chi_i \theta_{i-1}(\eta)] &= \hbar_\theta \mathcal{R}_{\theta,i}(\eta), \\ \mathcal{L}_\phi[\phi_i(\eta) - \chi_i \phi_{i-1}(\eta)] &= \hbar_\phi \mathcal{R}_{\phi,i}(\eta), \end{aligned}\right\} \tag{5.4.19}$$

and

$$f_i(0) = f_i'(0) = \phi'(0) = \theta'(0) = 0, f_i'(\infty) = \phi(+\infty) = 0, \theta(+\infty) = 0. \quad (5.4.20)$$

where

$$\begin{aligned}\mathcal{R}_{f,i}(\eta) = f_{i-1}''' &- 3\zeta\left(\frac{p_i-1}{2}\right)We^2\sum_{j=0}^{i-1}f_{i-1-j}'''\sum_{l=0}^{j}f_{j-l}''\sum_{p=0}^{l}f_p''\theta_{l-p} \\ &- \zeta\sum_{j=0}^{i-1}f_{i-1-j}''\theta_j' - \zeta\left(\frac{p_i-1}{2}\right)We^2\sum_{j=0}^{i-1}f_{i-1-j}'''\sum_{l=0}^{j}f_{j-l}''\sum_{p=0}^{l}f_p''\theta_{l-p}' \\ &+ M^2(1-f_{i-1}') + m\left(1-\sum_{j=0}^{i-1}f_{i-1-j}'f_j'\right) + \left(\frac{m+1}{2}\right)\sum_{j=0}^{i-1}f_{i-1-j}f_j'' \quad (5.4.21)\end{aligned}$$

$$\begin{aligned}\mathcal{R}_{\theta,\,i}(\eta) = &\frac{4}{3}Rd(\theta_w-1)^3\left\{\sum_{j=0}^{i-1}\theta_{i-1-j}''\sum_{l=0}^{j}\theta_{j-l}\sum_{p=0}^{l}\theta_{l-p}\theta_p\right\} + \left(1+\frac{4}{3}Rd\right)\theta_{i-1}'' \\ &+ 4Rd(\theta_w-1)^3\left\{\sum_{j=0}^{i-1}\theta_{i-1-j}'\sum_{l=0}^{j}\theta_{j-l}'\sum_{p=0}^{l}\theta_{l-p}\theta_p\right\} + DuPr\phi_{i-1}'' \\ &+ 4Rd(\theta_w-1)\sum_{j=0}^{i-1}\theta_{i-1-j}''\theta_j + 4Rd(\theta_w-1)^2\sum_{j=0}^{i-1}\theta_{i-1-j}''\sum_{l=0}^{j}\theta_{j-l}\theta_l \\ &+ 4Rd(\theta_w-1)\sum_{j=0}^{i-1}\theta_{i-1-j}'\theta_j' + 8Rd(\theta_w-1)^2\sum_{j=0}^{i-1}\theta_{i-1-j}'\sum_{l=0}^{j}\theta_{j-l}'\theta_l \\ &+ Pr\left(\frac{m+1}{2}\right)\sum_{j=0}^{i-1}\theta_{i-1-j}'f_j, \quad (5.4.22)\end{aligned}$$

$$\mathcal{R}_{\phi,i}(\eta) = \phi_{i-1}'' + \left(\frac{m+1}{2}\right)Sc\sum_{j=0}^{i-1}f_j\phi_{i-1-j}' + SrSc\theta_{i-1}'', \quad (5.4.23)$$

with

$$\chi_i = \begin{cases}0, & i<1\\ 1, & i\geq 1\end{cases} \quad (5.4.24)$$

The general solutions of Equation (5.4.19) are given by,

$$f_i(\eta) = f_i^*(\eta) + k_1 + k_2\eta + k_3e^{-\eta}, \quad (5.4.25)$$

$$\theta_i(\eta) = \theta_i^*(\eta) + k_4 + k_5e^{-\eta}, \quad (5.4.26)$$

$$\phi_i(\eta) = \phi_i^*(\eta) + k_6 + k_7e^{-\eta}, \quad (5.4.27)$$

where the constants $k_j, (j = 1, 2, \ldots, 7)$ can be found by the boundary conditions.

Table 5.1: Comparison of numerical and analytical outcomes when $We = 0.05, p_i = 0.2, M = 0.04, f_w = 0.4, m = 0.6, Pr = 0.7, \zeta = 0.4, B = 0.5$ for various values of η.

	HAM	Solution	[Present]			BVP 4C	[128]	
η	f	f'	$-\theta'$	ϕ	f	f'	$-\theta'$	ϕ
0.0000	0.4000	0.5000	1.0000	1.0000	0.4000	0.5000	1.0000	1.0000
0.0045	0.4023	0.5038	0.9990	0.9984	0.4023	0.5035	0.9990	0.9984
0.0090	0.4045	0.5076	0.9981	0.9968	0.4045	0.5070	0.9981	0.9968
0.0135	0.4068	0.5114	0.9971	0.9952	0.4068	0.5105	0.9971	0.9952
0.0180	0.4091	0.5151	0.9961	0.9936	0.4091	0.5139	0.9961	0.9936
0.0225	0.4115	0.5180	0.9951	0.9921	0.4115	0.5174	0.9951	0.9921
0.0270	0.4138	0.5226	0.9941	0.9905	0.4138	0.5208	0.9941	0.9905
0.0315	0.4161	0.5263	0.9931	0.9889	0.4161	0.5242	0.9931	0.9889
0.0360	0.4185	0.5300	0.9921	0.9873	0.4185	0.5275	0.9921	0.9873
0.0405	0.4209	0.5336	0.9911	0.9857	0.4209	0.5309	0.9911	0.9857
0.0450	0.4233	0.5373	0.9901	0.9841	0.4233	0.5342	0.9901	0.9841

5.5 Convergence Analysis

For the appropriate choice of $\hbar_f$, $\hbar_\theta$ and $\hbar_\phi$ HAM solutions converges. $f''(1)$, $\theta'(1)$ and $\phi'(1)$ are plotted upto the suitable approximations. We can choose $\hbar_f = -0.4$, $\hbar_\theta = -0.5$ and $\hbar_\phi = -1.0$ from Figure 5.1.

5.6 Result and discussion

To gain a clear physical understanding of the current problem, computations for variations in the pertinent parameters are performed using the Mathematica software, and the results are graphically illustrated in Figures 5.2 - 5.22. Comparison of the current outcome and available published outcome using BVP 4C by Abbas et al. [128] are given in Table 5.1 and Table 5.2, for the purpose of verifying the accuracy of the used HAM. The comparision contains agreement. As a result, we are sure that the existing results are accurate.

Figure 5.2 illustrates similar behaviour for variable viscosity parameter ζ on velocity profile $f'(\eta)$ with shrinking and stretching parameter B. With increasing values of ζ, $f'(\eta)$ increases. Opposite behaviour for M on $f'(\eta)$ in the shrinking and stretching case can be viewed in Figure 5.3. When M increases, $f'(\eta)$ increases for shrinking parameter and decreases for stretching parameter while the other parameters are kept fixed. Lorentz force opposes the pressure acting on the opposite direction of the fluid flow. Here friction force slows fluid's movement. Figure 5.4

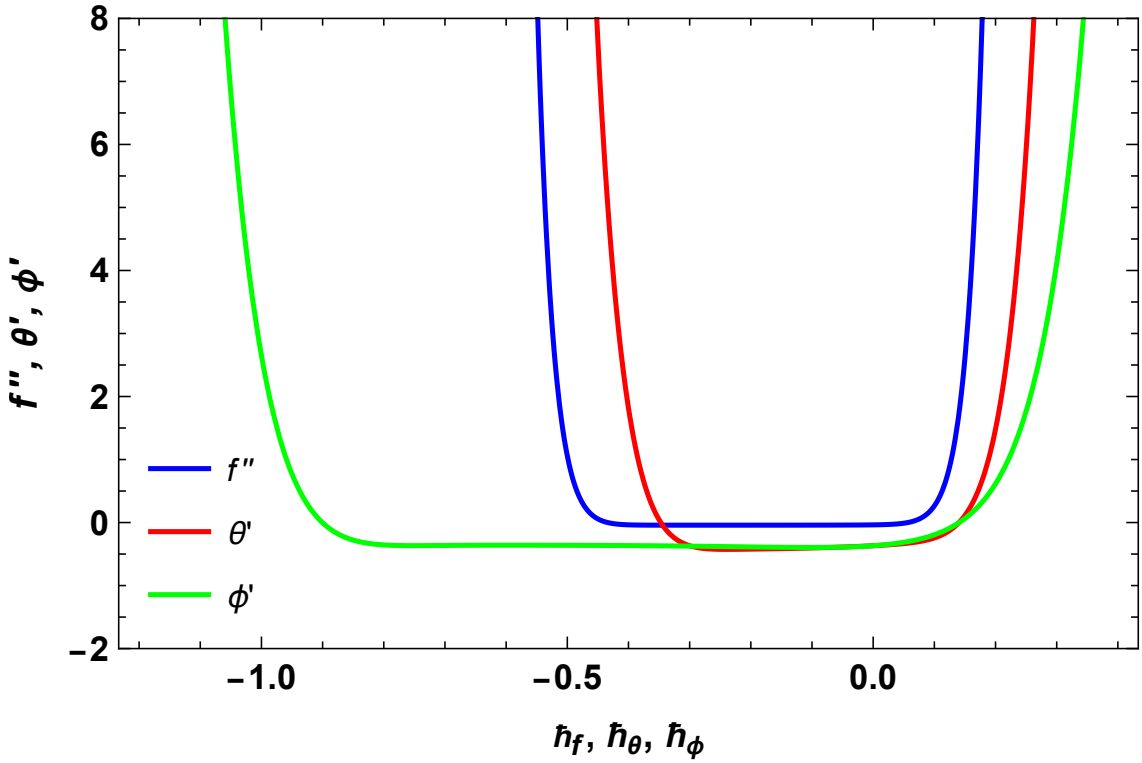

Figure 5.1: $\hbar$-curve for range f'', θ' and ϕ'.

scrutinized effect of m on $f'(\eta)$. It shows that $f'(\eta)$ enhances with m for the both shrinking/stretching cases. The consequences of p_i on the $f'(\eta)$ is depicted in Figure 5.5. For $B < 0$, $f'(\eta)$ decreases while increases for $B > 0$. Figure 5.6 examined effect of f_w on the $f'(\eta)$, when the other parameters are held constant, for increasing values of f_w, $f'(\eta)$ increases in both shrinking and stretching. Figure 5.7 depicts the impact of We on the $f'(\eta)$. In the case of shrinking, $f'(\eta)$ raises with a rise in We, whereas the reverse sort of behaviour has been witnessed in the case of stretching.

The consequence of M on $\theta(\eta)$ is depicted in Figure 5.8. A rise in M has been evidenced to raise $\theta(\eta)$. Figure 5.9 shows that $\theta(\eta)$ declined for a large amount of m. The impact of Rd on $\theta(\eta)$ is demonstrated in Figure 5.10. It is worth noting that the $\theta(\eta)$ increased for large values of Rd. The impact of θ_w on $\theta(\eta)$ is explained in Figure 5.11. We can see that for large values of θ_w, $\theta(\eta)$ rises. The variation of various values of Du on $\theta(\eta)$ is depicted in Figure 5.12. It is discovered that the diffusion thermal effect has a significant impact on fluid temperature. For increasing values of Du, $\theta(\eta)$ increases. Figure 5.13 demonstrates how Sc influences $\phi(\eta)$. A reduction in $\phi(\eta)$ is encountered with increasing values of Sc, mass diffusivity decreases. The variation of different values of Sr on $\phi(\eta)$ is depicted in Figure 5.14. $\phi(\eta)$ rises as the value of Sr rises.

Figures 5.15 and 5.16 demonstrate the trend of S on friction factor for shrinking

Table 5.2: Comparison of numerical and analytical outcomes when $We = 0.5, p_i = 0.2, M = 0.04, f_w = 0.4, m = 0.6, Pr = 2, \zeta = 0.4, B = 0.5$ for various values of η.

	HAM	Solution	[Present]			BVP 4C	[128]	
η	f	f'	$-\theta'$	ϕ	f	f'	$-\theta'$	ϕ
0.0000	0.4000	0.5000	1.0000	1.0000	0.4000	0.5000	1.0000	1.0000
0.0015	0.4008	0.5012	0.9991	0.9995	0.4008	0.5012	0.9991	0.9995
0.0030	0.4015	0.5024	0.9981	0.9989	0.4015	0.5024	0.9981	0.9989
0.0045	0.4023	0.5037	0.9972	0.9984	0.4023	0.5036	0.9972	0.9984
0.0060	0.4030	0.5049	0.9962	0.9979	0.4030	0.5048	0.9962	0.9979
0.0075	0.4038	0.5062	0.9953	0.9974	0.4038	0.5060	0.9953	0.9974
0.0090	0.4045	0.5074	0.9943	0.9968	0.4045	0.5072	0.9943	0.9968
0.0105	0.4053	0.5086	0.9934	0.9963	0.4053	0.5084	0.9934	0.9958
0.0120	0.4061	0.5099	0.9924	0.9958	0.4061	0.5096	0.9924	0.9958
0.0135	0.4068	0.5111	0.9914	0.9952	0.4068	0.5108	0.9914	0.9952
0.0150	0.4076	0.5123	0.9905	0.9947	0.4076	0.5120	0.9905	0.9947

cases in 2-dimensions and 3-dimensions. Friction factor enhances as S rises in the shrinking case, and the reverse trend can be spotted in Figures 5.17 and 5.18 for the stretching case in 2-dimensions and 3-dimensions. Figure 5.19 and 5.20 display the effect of θ_w on the Nusselt count in 2-dimensions and 3-dimensions, respectively. The Nusselt count is rising for θ_w. Figure 5.21 and 5.22 demonstrate the trend of Sr on Sherwood count in 2-dimensions and 3-dimensions respectively. Sherwood count rises as Sr boosts. The numerical output of skin friction and the Nusselt count are described in Table 5.3 and 5.4.

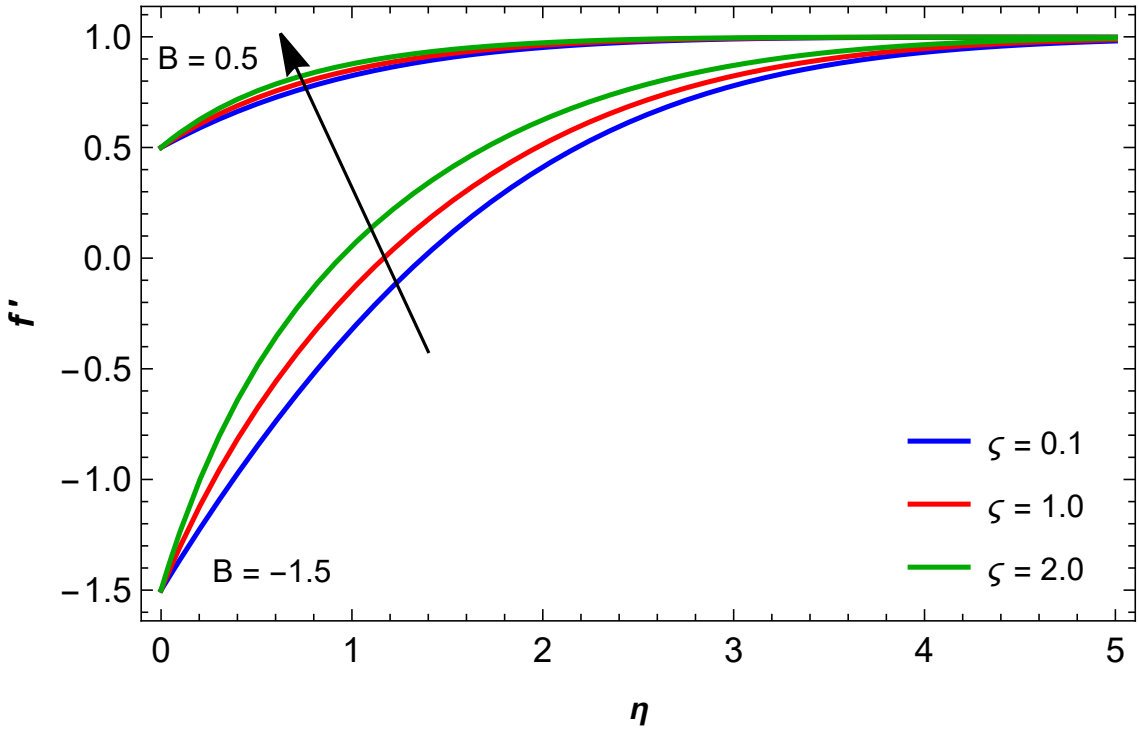

Figure 5.2: f' via ζ

Table 5.3: Comparison of Skin friction for stretching/shrinking case and different values of p_i, f_w, m, M, ζ.

p_i	m	ζ	M	f_w	$Cf_x Re_x^{\frac{1}{2}}$ for $B = -2.0$	$Cf_x Re_x^{\frac{1}{2}}$ for $B = 2.0$
1.0	0.1	0.1	0.1	0.1	1.3657	-0.9071
2.0					1.3843	-0.9219
3.0					1.3933	-0.9365
	0.1				1.3657	-0.9071
	0.2				1.3926	-1.0195
	0.3				1.4194	-1.1326
		0.1			1.3657	-0.9071
		0.2			1.0656	-0.7448
		0.3			0.7147	-0.5689
			0.1		1.3657	-0.9071
			0.2		1.3939	-0.9170
			0.3		1.4409	-0.9334
				0.1	1.3657	-0.9071
				0.2	1.4211	-0.9275
				0.3	1.4767	-0.9480

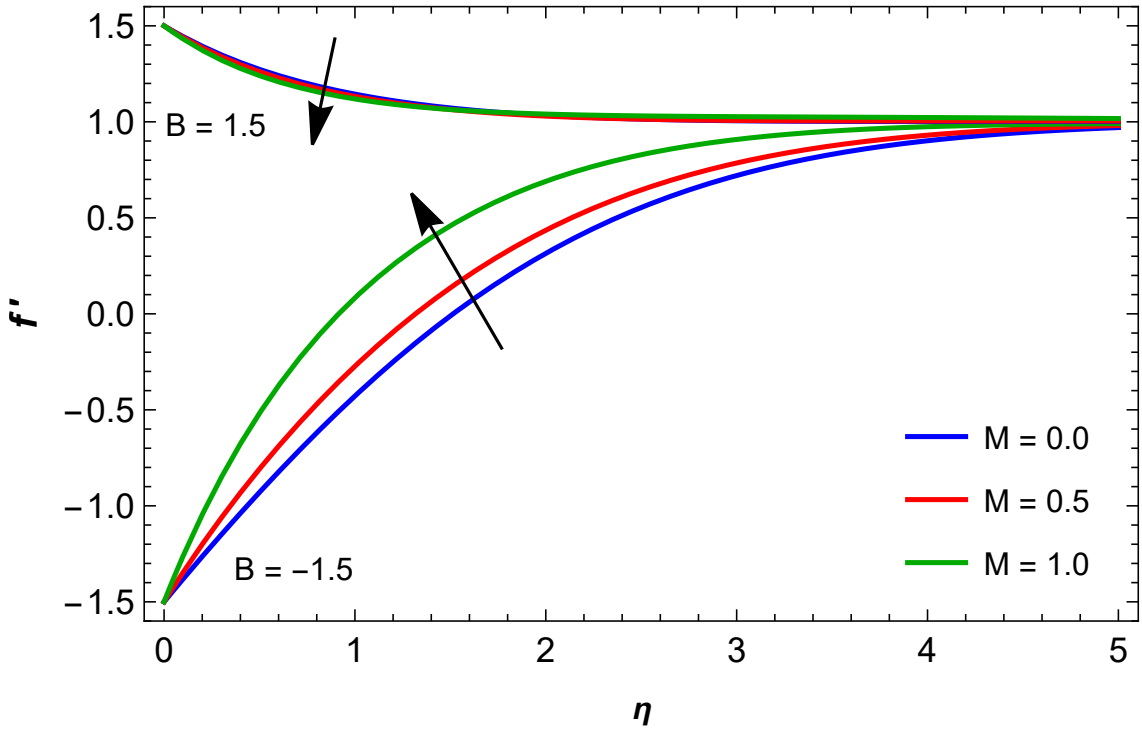

Figure 5.3: f' via M

Table 5.4: Nusselt count for different values of Pr, Du, m, Rd, θ_w.

Pr	Du	m	Rd	θ_w	$Nu_x Re_x^{\frac{-1}{2}}$.
7.0	0.01	0.1	0.5	0.9	-3.4411
8.0					-2.1908
9.0					-1.6450
	0.01				-3.4411
	0.02				-3.6896
	0.03				-3.9798
		0.1			-3.4411
		0.2			-2.5031
		0.3			-1.9908
			0.5		-3.4411
			0.6		-4.1257
			0.7		-4.9698
				0.9	-3.4411
				1.0	-3.9633
				1.1	-5.2880

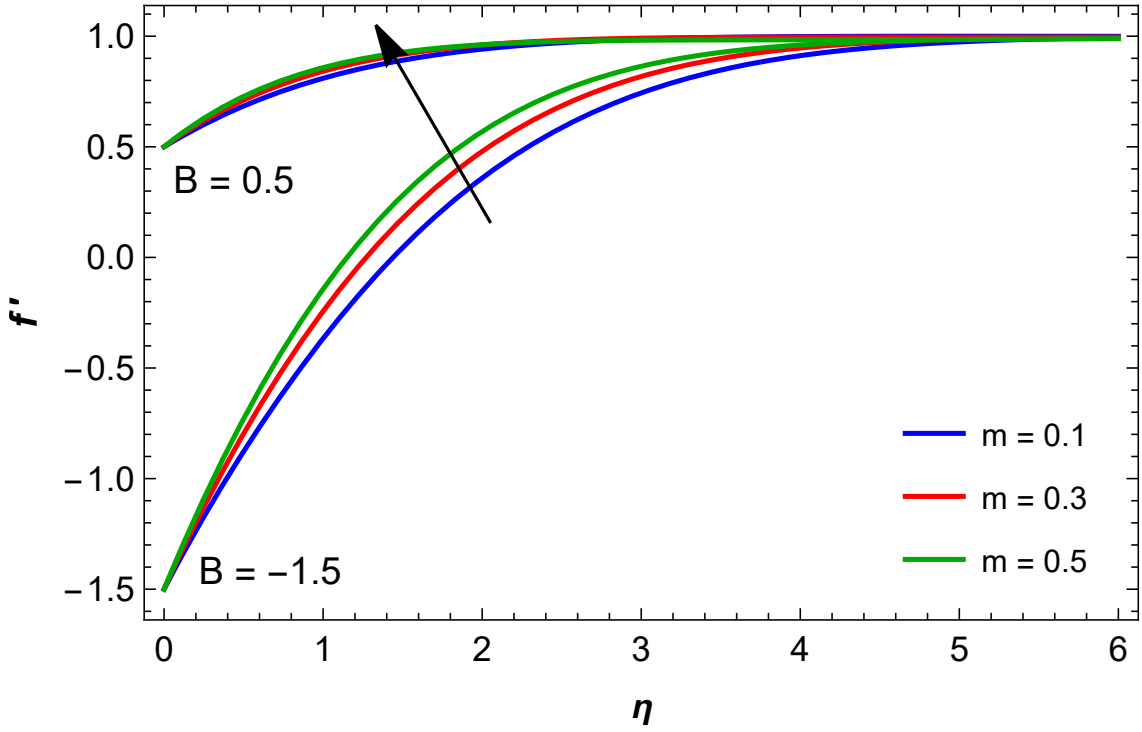

Figure 5.4: f' via m

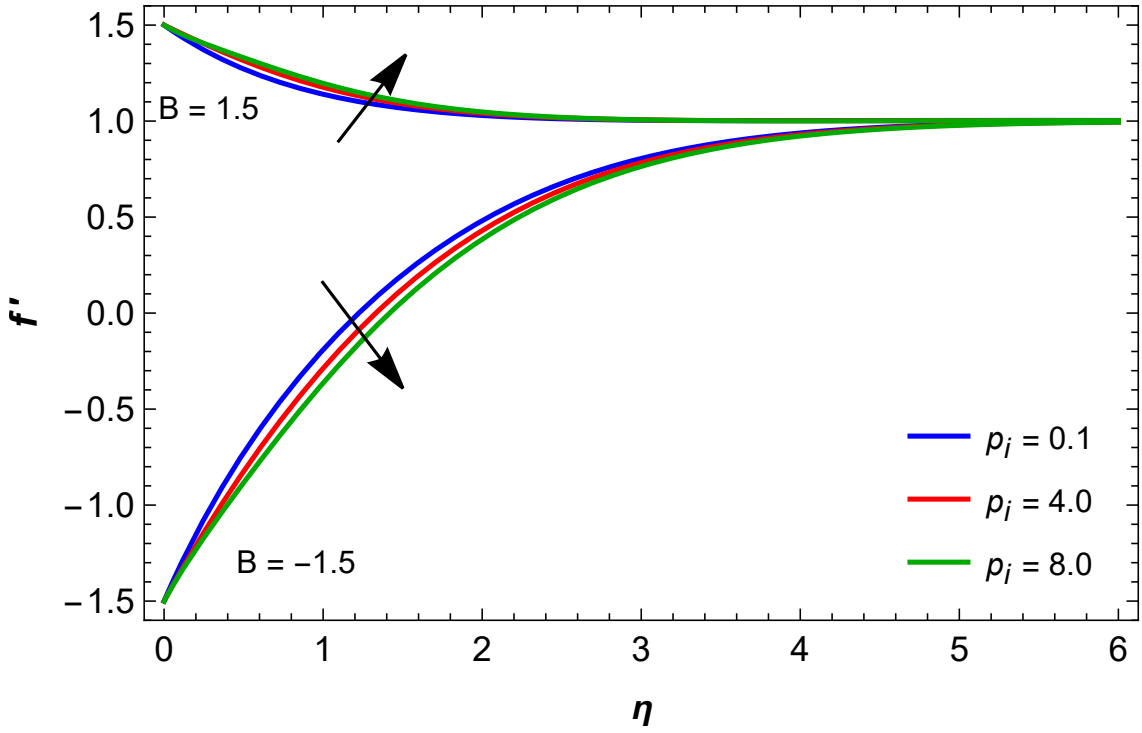

Figure 5.5: f' via p_i

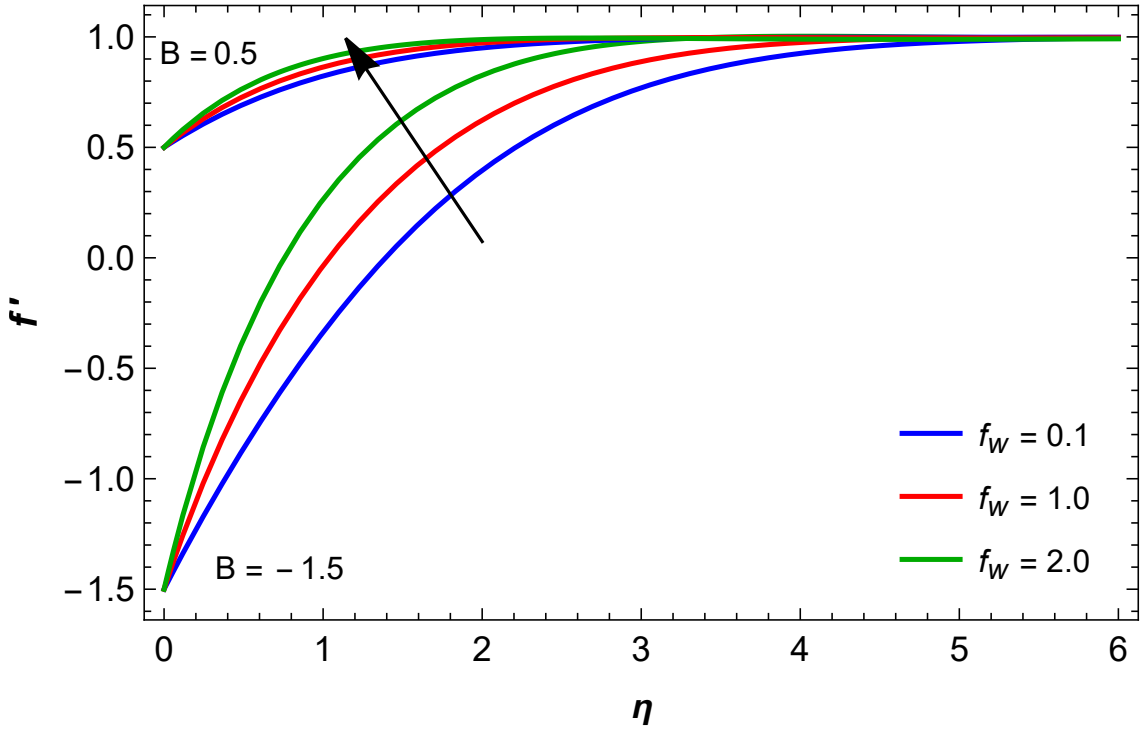

Figure 5.6: f' via f_w

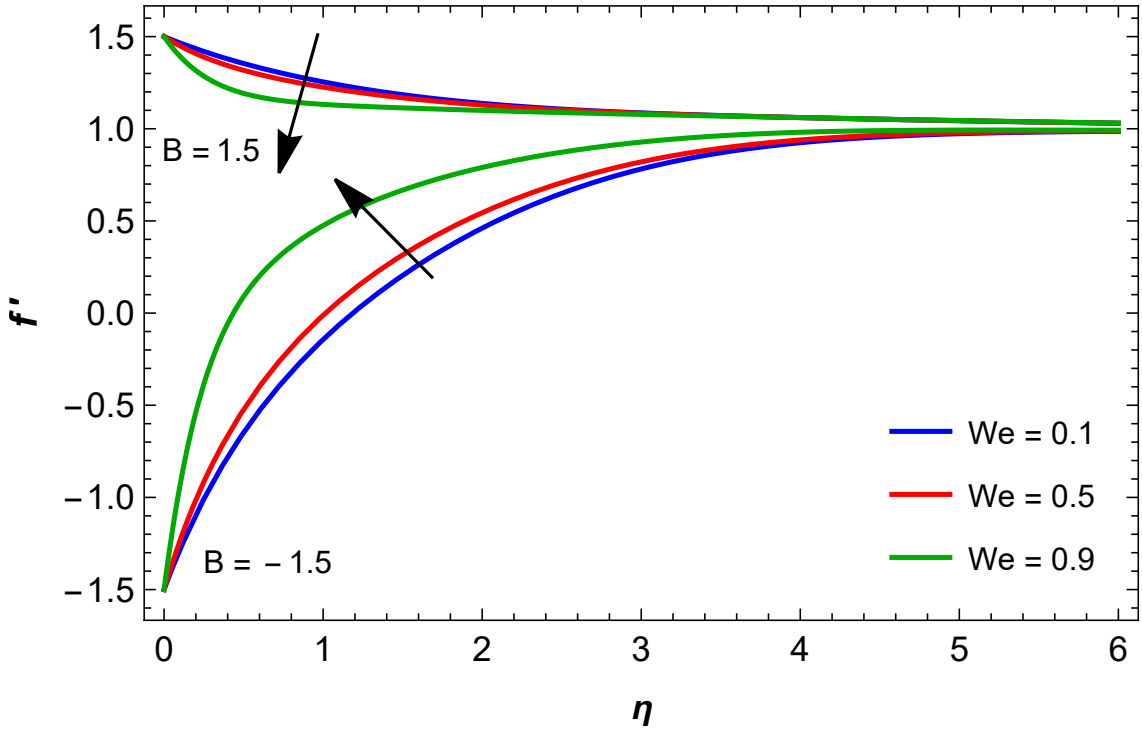

Figure 5.7: f' via We

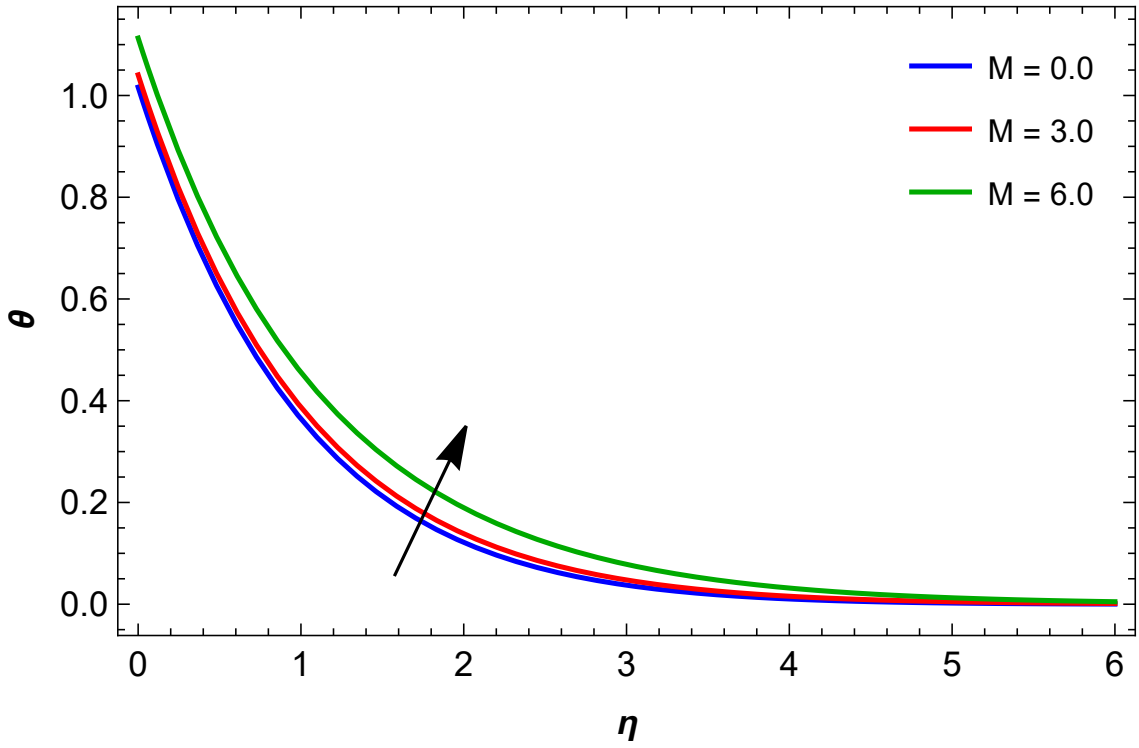

Figure 5.8: θ via M

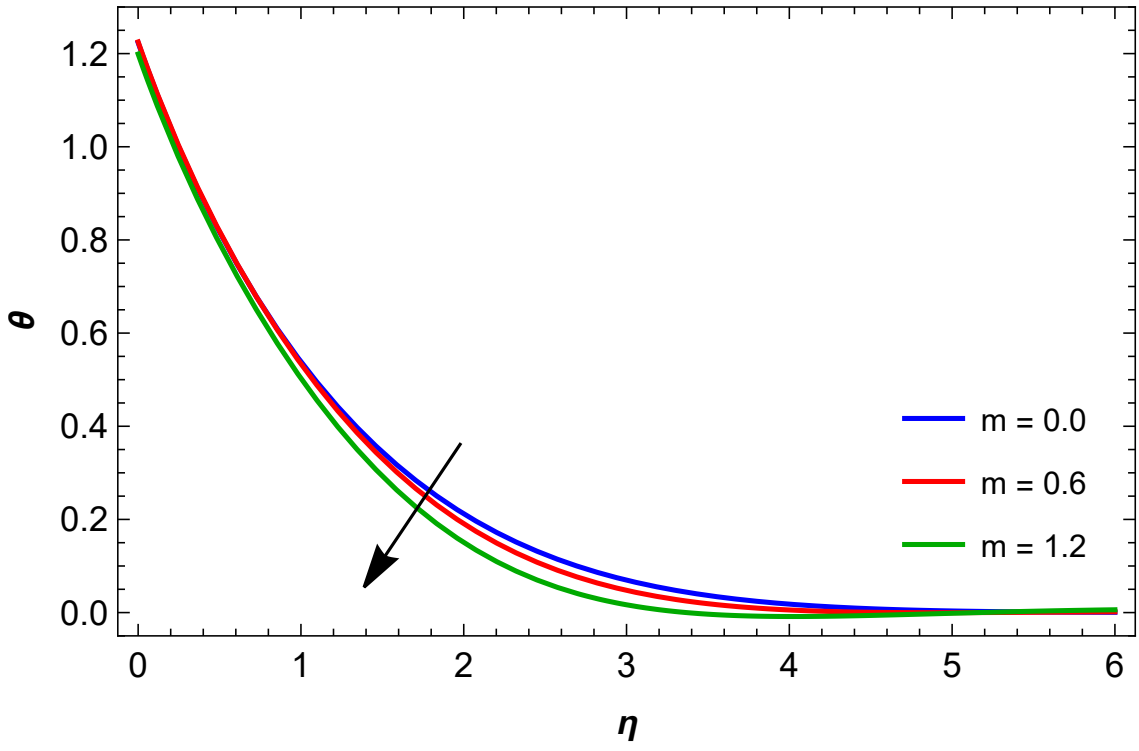

Figure 5.9: θ via m

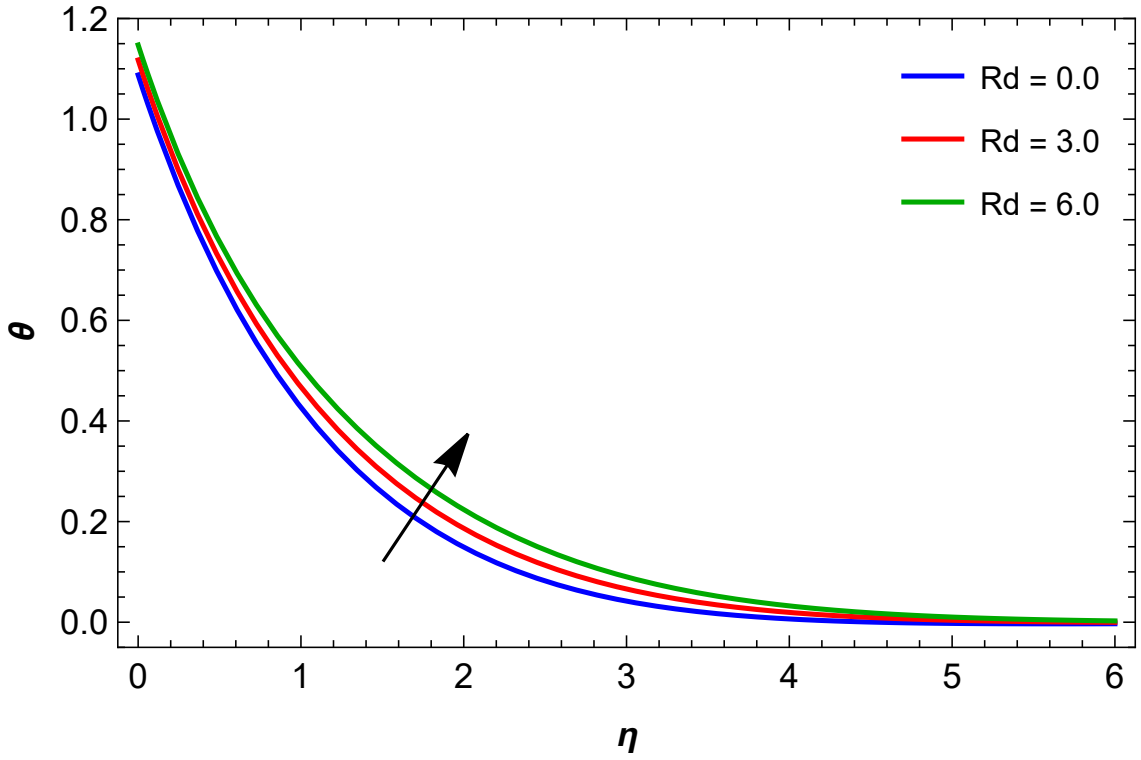

Figure 5.10: θ via Rd

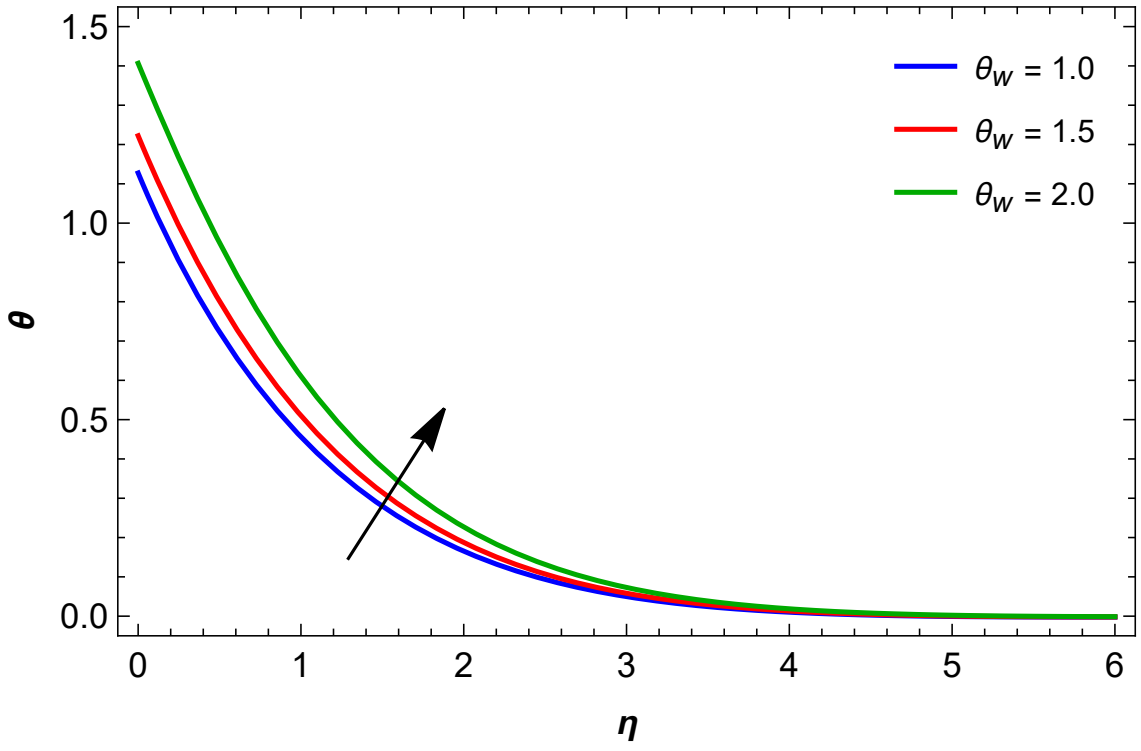

Figure 5.11: θ via θ_w

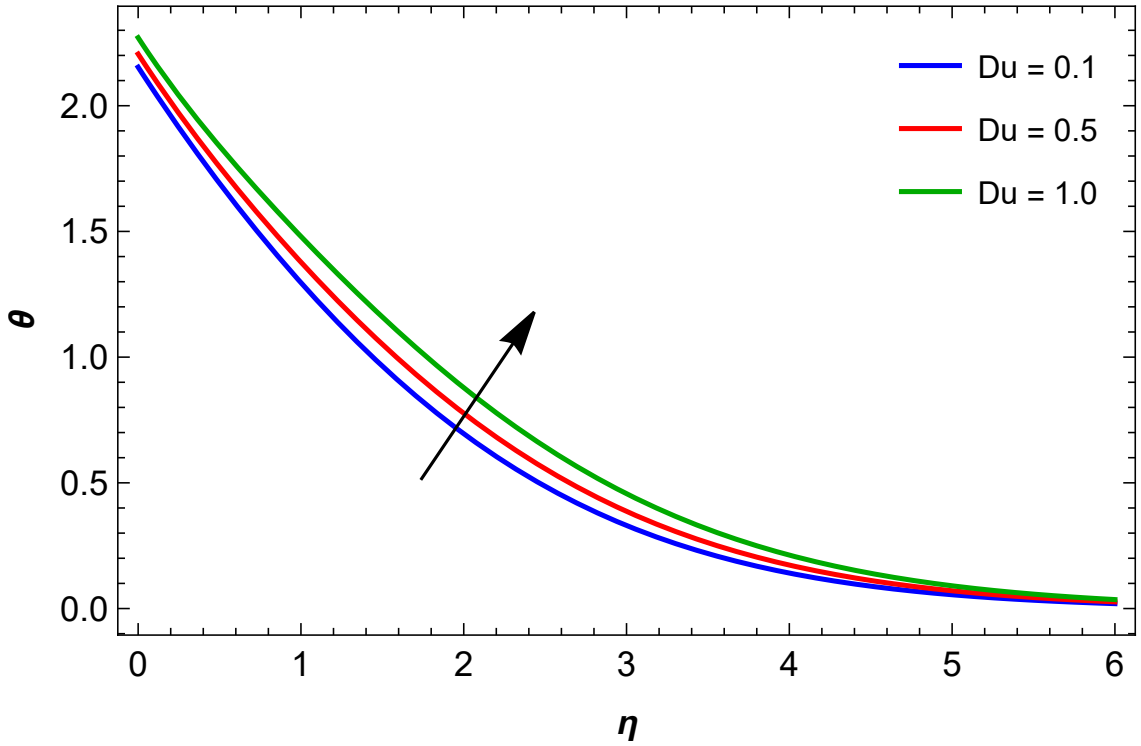

Figure 5.12: θ via Du

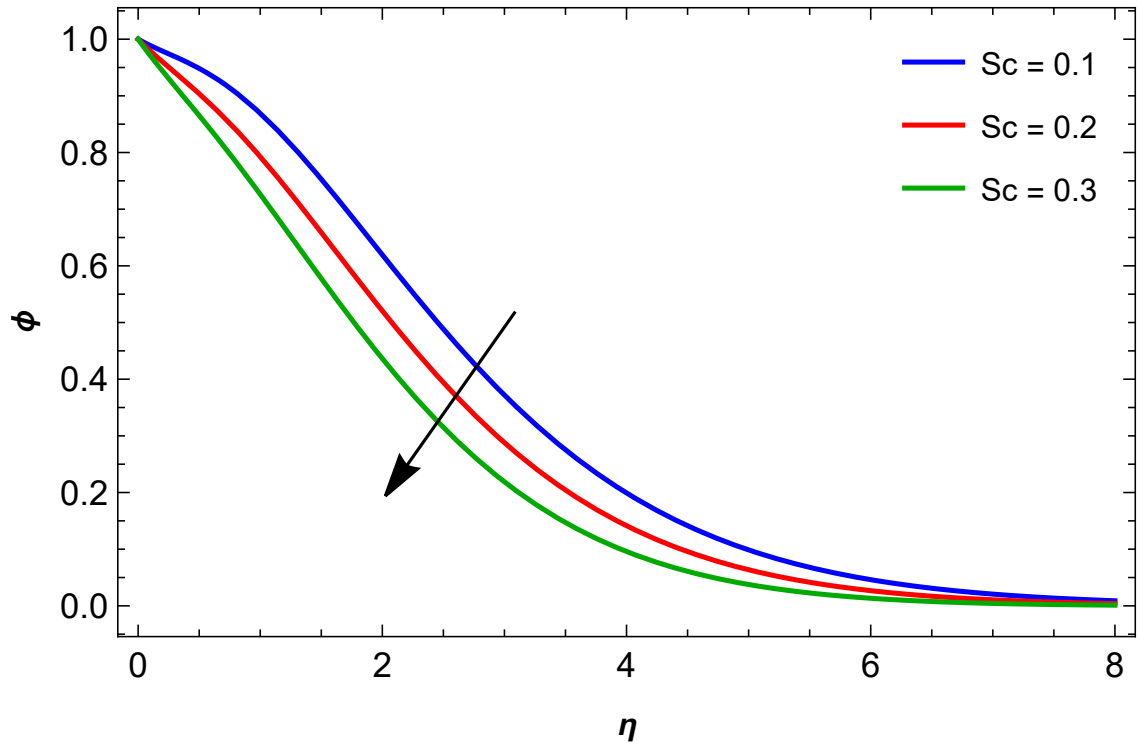

Figure 5.13: ϕ via Sc

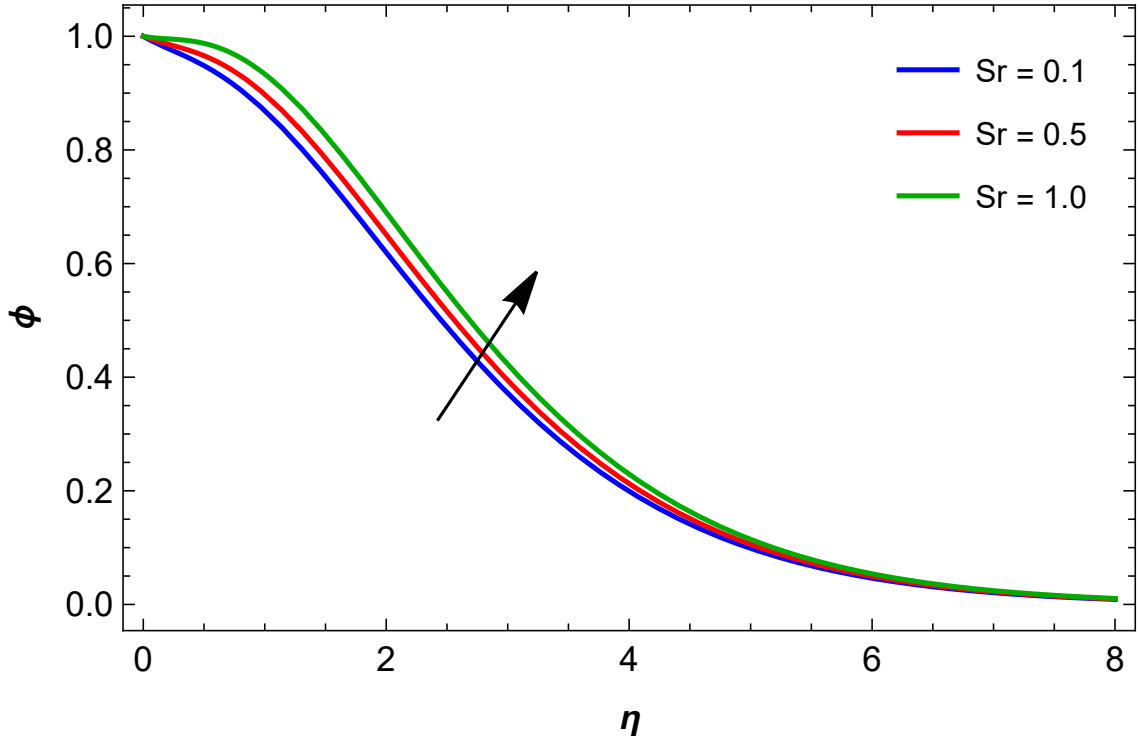

Figure 5.14: ϕ via Sr

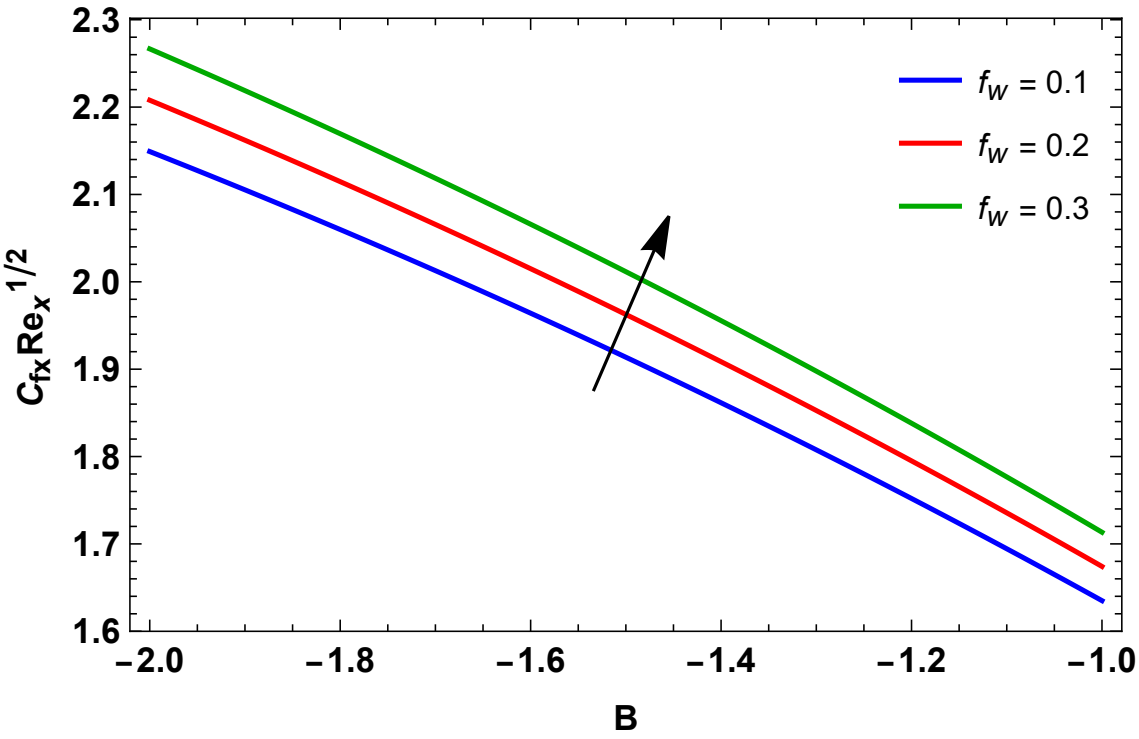

Figure 5.15: Friction factor for f_w in 2-dimension shrinking case

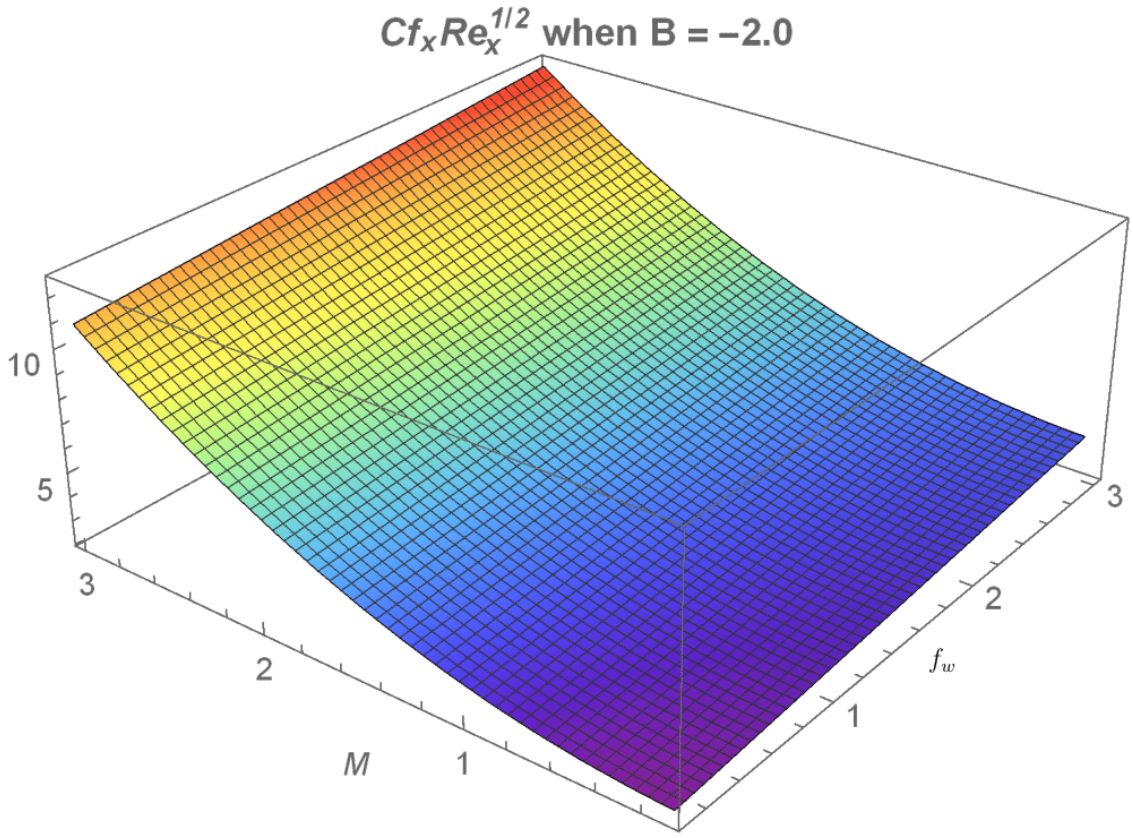

Figure 5.16: Friction factor for f_w in 3-dimension shrinking case

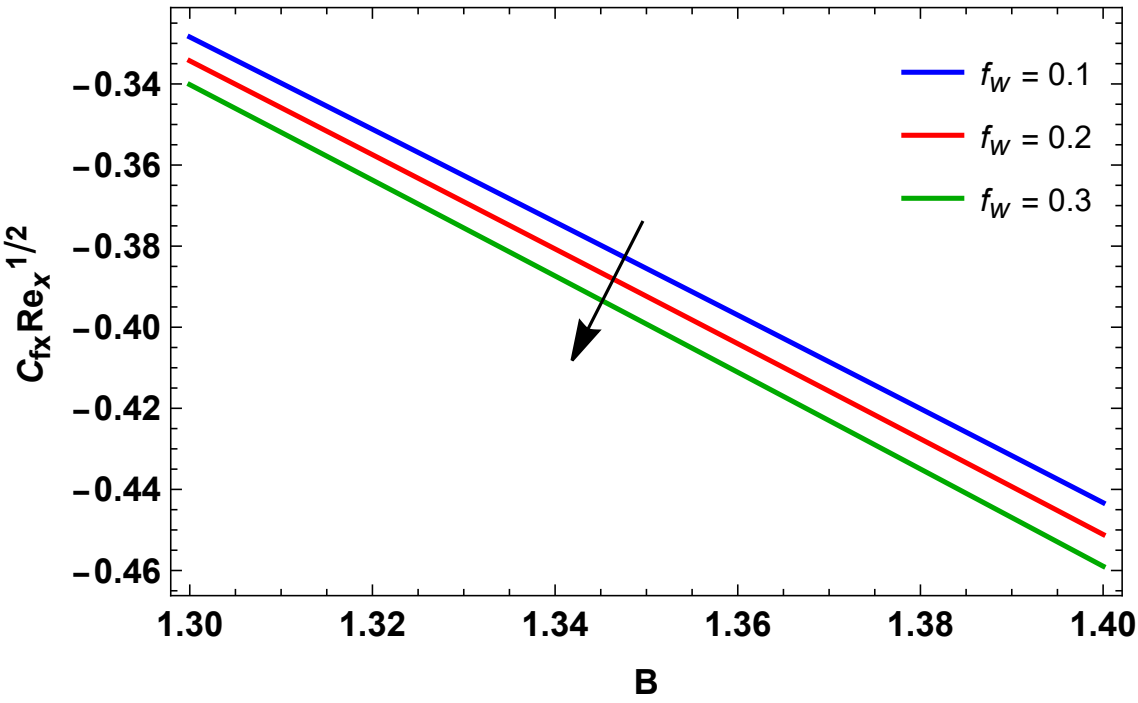

Figure 5.17: Friction factor for f_w in 2-dimension stretching case

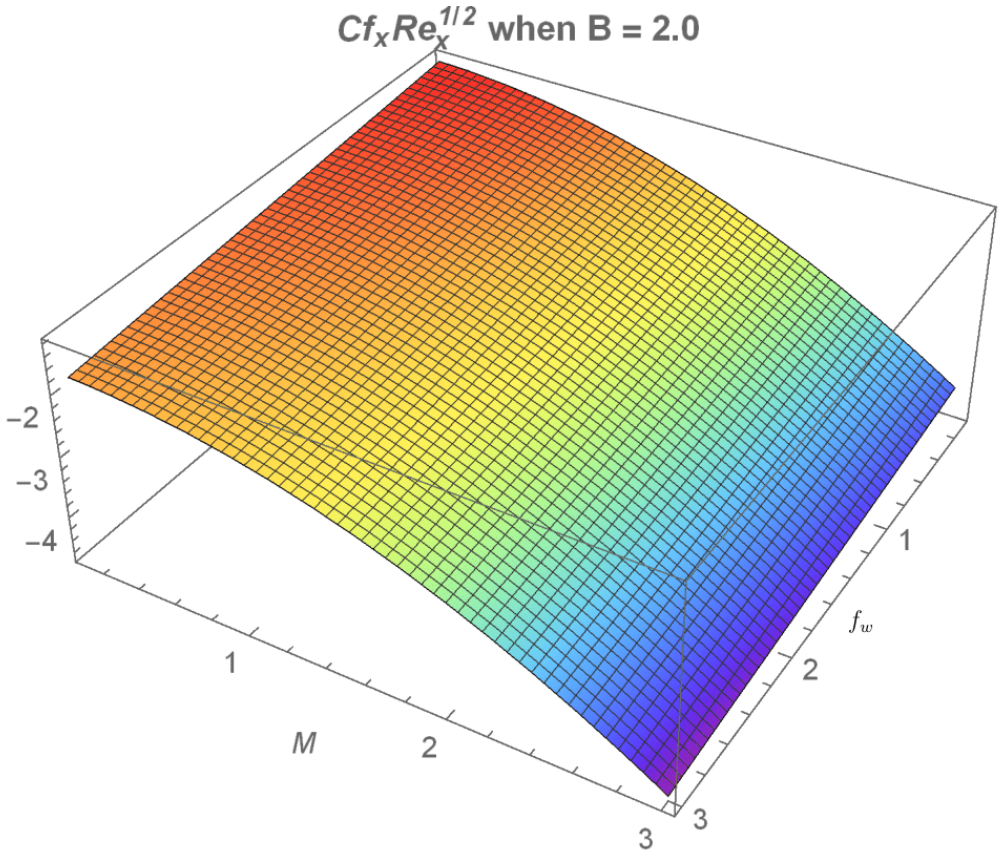

Figure 5.18: Friction factor for f_w in 3-dimension stretching case

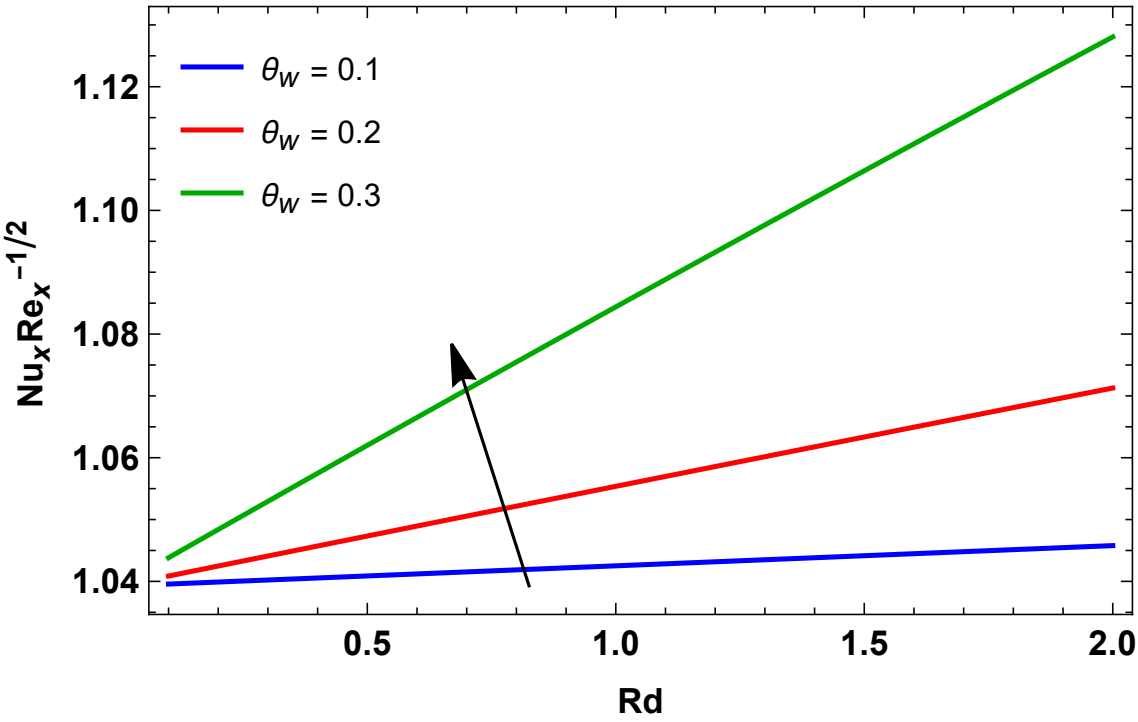

Figure 5.19: Nusselt count for Rd and θ_w

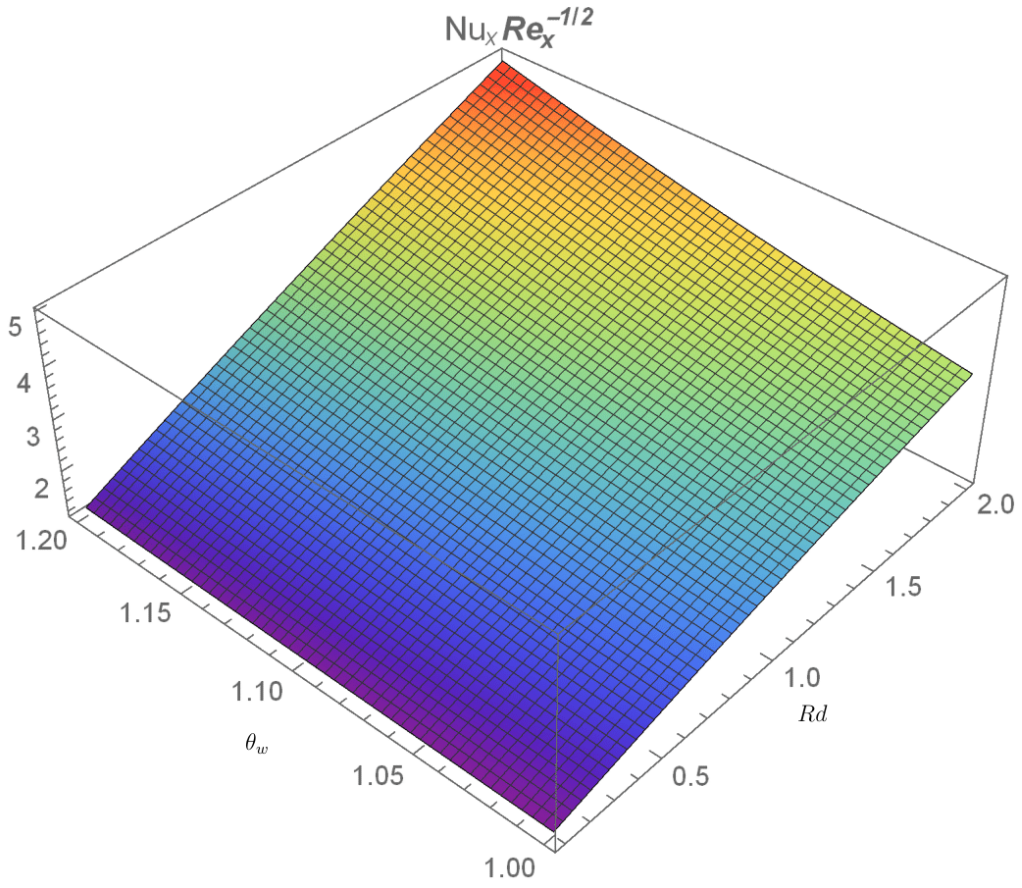

Figure 5.20: Nusselt count for Rd and θ_w

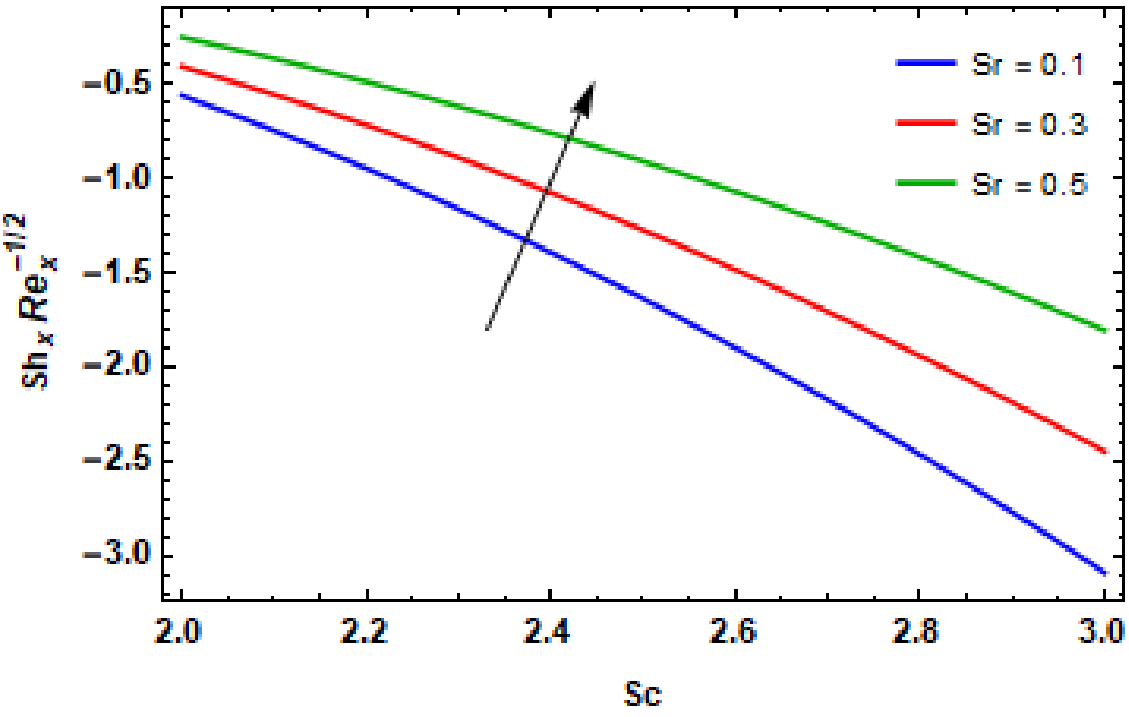

Figure 5.21: Sherwood count for Sc and Sr

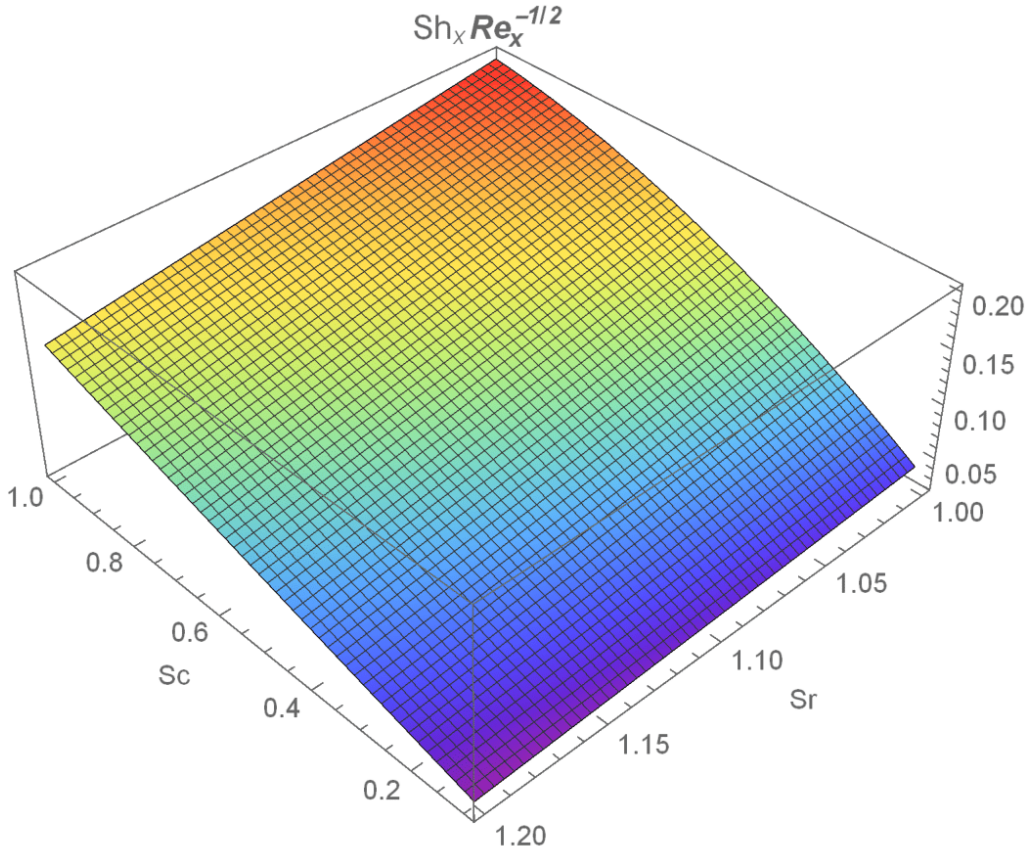

Figure 5.22: Sherwood count for Sc and Sr

5.7 Conclusion

The main findings of the research are following:

- Velocity field increases for variable viscosity parameter, Nonlinear parameter and Suction parameter for shrinking and stretching cases.
- For large amount of Magnetic parameter and Weissenberg number velocity field increases in shrinking case and behaves opposite in stretching case.
- For large value of power index, velocity decreases in shrinking case and reverse effect ouccurs for stretching case.
- Temperature enhances for large amount of Magnetic parameter, Temperature ratio parameter, Dufour number and Radiation parameter, and gives reverse impact for nonlinear parameter.
- Concentration field increases for Soret number and behaves opposite for Schimdt number.
- Skin friction coefficient increases with increaseing values of Suction parameter for shrinking case and decreasing for stretching case.
- Nusselt count increases for large amount of temperature ratio parameter.
- For increasing values of Soret number, Sherwood count increases.